

# Rate-Dependent Decohesion Modes in Graphene-Sandwiched Interfaces

Chaochen Xu, Tianhao Yang, Yilan Kang, Qunyang Li, Tao Xue, Kenneth M. Liechti, Rui Huang,\* and Wei Qiu\*

Mechanical dry transfer of large-area graphene is increasingly applied in fabrication of graphene-based electronic devices, and adhesion energy of graphene/substrate interface is a key factor affecting reliability and performance of these devices. Herein, the adhesion energy of a graphene/poly(ethylene terephthalate) (PET) interface is measured by widely adopted double cantilever beam (DCB) fracture tests. Results show that the apparent adhesion energy of sandwiched interface is highly rate-dependent. When separation rate increases from 20 to 150  $\mu\text{m s}^{-1}$ , apparent adhesion energy increases by an order of magnitude. By examining fractured interfaces after DCB tests with micro-Raman spectroscopy, the graphene is found to be fractured and transferred in fragments, with residual tensile strain up to 3% for high separation rates. The results are contrary to earlier reports, where higher separation rate in dry-transfer process would typically enhance the dry transfer of graphene, resulting in better integrity and performance. Based on Raman spectroscopy measurements, three distinct decohesion modes are identified for PET-/graphene-/adhesive-sandwiched interface, which consistently explain the rate-dependent apparent adhesion energy. The complicated decohesion modes also suggest that an optimal separation rate should be used to properly measure the adhesion energy and improve the dry-transfer technique of graphene with minimum damage and residual strain.

## 1. Introduction

Practical industrial mass production of macrosized graphene has been realized with the development of the chemical vapor deposition (CVD) method, envisioning a wide range of potential applications in microelectronic devices.<sup>[1–3]</sup> However, as a key step in the fabrication process, the successful transfer of high-quality macrosized graphene to a specific target substrate of these devices continues to be a challenge. Compared with the typical transfer method of graphene, which often involves wet chemical etching, the etching-free mechanical dry-transfer process is fast, renewable, cost-competitive, and environmentally friendly.<sup>[4,5]</sup> The adhesion energy of graphene to various substrate materials, as a key parameter characterizing the mechanical resistance to delamination of the graphene/substrate interface, has been shown to be a critical factor determining the quality of the transferred graphene and the performance of graphene-based devices.<sup>[5]</sup> Therefore, the development of an appropriate method

for measuring the adhesion energy of the graphene/substrate interface is essential for large-scale fabrication and device applications of graphene.


In the last decade, significant progress has been made in experimental investigations characterizing the interfacial properties of graphene using the shear-lag method,<sup>[6–10]</sup> the blister tests,<sup>[11–16]</sup> the double cantilever beam (DCB) fracture tests,<sup>[5,17,18]</sup> and nanoindentation methods.<sup>[19,20]</sup> Shear-lag methods are often employed to study sliding and shear interactions of the graphene/substrate interfaces, whereas the adhesion energy is typically measured using the DCB and blister tests. For experimental investigation of the adhesive interactions, Koenig et al.<sup>[11]</sup> performed a pressurized blister test by creating a pressure difference across the graphene membrane to directly measure the adhesion energy between graphene and a silicon-oxide substrate and obtained a value of  $\Gamma_{\text{g/Si}} = 0.45 \pm 0.02 \text{ J m}^{-2}$ , whereas Wang et al.<sup>[12]</sup> used the same method to obtain a smaller value of  $\Gamma_{\text{g/Si}} = 0.19 \pm 0.02 \text{ J m}^{-2}$ . Recently, Xin et al.<sup>[13]</sup> measured the adhesion energy of the as-grown graphene on copper foil of different roughness using a blister test and obtained values

Dr. C. Xu, Prof. Y. Kang, Prof. W. Qiu  
Tianjin Key Laboratory of Modern Engineering Mechanics  
School of Mechanical Engineering  
Tianjin University  
Tianjin 300072, P. R. China  
E-mail: qiuwei@tju.edu.cn

Dr. C. Xu, Prof. Q. Li  
Applied Mechanics Laboratory  
Department of Engineering Mechanics  
Tsinghua University  
Beijing 100084, P. R. China

T. Yang, Prof. K. M. Liechti, Prof. R. Huang  
Department of Aerospace Engineering and Engineering Mechanics  
University of Texas at Austin  
Austin, TX 78712, USA  
E-mail: ruihuang@mail.utexas.edu

Dr. T. Xue  
Center for Analysis and Test  
Tianjin University  
Tianjin 300072, P. R. China

 The ORCID identification number(s) for the author(s) of this article can be found under <https://doi.org/10.1002/admi.201901217>.

DOI: 10.1002/admi.201901217

ranging between 0.61 and 1.64 J m<sup>-2</sup>. They observed that the surface roughness of the substrate was an important factor in determining the adhesion energy, with rougher copper foil surfaces leading to higher adhesion energy. However, these blister tests were restricted to the measurement of the adhesion energy of micro-sized graphene. For large area graphene, blister tests were applied in conjunction with a backing layer to support the graphene.<sup>[14–16]</sup> In either case, the combination of tension and shear at the interface in the blister tests introduces a mixed-mode effect on adhesion that has to be carefully accounted for.

For measurement of the adhesion energy of large-sized graphene prepared using CVD, the DCB method is often employed. The first step of the DCB method is to prepare a DCB specimen by inserting the graphene-coated substrate between stiff materials such as silicon or glass strips using an adhesive to form a substrate/graphene/adhesive/substrate sandwich structure. Next, the DCB specimen is subjected to an opening load (or displacement) to peel graphene off the substrate by propagating a nominally mode-I crack along the graphene/substrate interface. The measured load–displacement response of the DCB specimen during the peeling process (dry transfer) can then be used to determine the adhesion energy of the graphene/substrate interface. Using this method, Yoon et al.<sup>[17]</sup> peeled off large-area monolayer graphene synthesized on a copper film at a separation rate of 5 μm s<sup>-1</sup>, and the adhesion energy of graphene and copper was determined to be  $\Gamma_{g/Cu} = 0.72 \pm 0.07$  J m<sup>-2</sup>. Na et al.<sup>[5]</sup> used a similar fracture test to determine the adhesion energy between graphene and its seed copper foil but observed that different separation rates led to different fracture paths and thus developed the selective dry-transfer method of graphene from one substrate to another. At a high separation rate of 254 μm s<sup>-1</sup>, graphene was completely transferred from the copper foil to the target substrate and an adhesion energy of  $\Gamma_{g/Cu} = 6$  J m<sup>-2</sup> was obtained, whereas a low separation rate of 25.4 μm s<sup>-1</sup> led to interfacial fracture along the graphene/adhesive interface with an adhesion energy of  $\Gamma_{g/epoxy} = 3.5$  J m<sup>-2</sup>. They attributed the observed selective fracture paths to two possible causes, one due to rate-dependent

adhesion–separation processes and the other due to the surface roughness of the substrate.

It can be observed from the previous works that the adhesion energy is an important parameter characterizing the strength of the graphene/substrate interface and that its characterization has widespread significance for the industrial production and transfer of graphene. Compared to the blister-test methods, the DCB method has the advantage of not relying on complex or costly experimental equipment such as atomic force microscopes or Raman spectrometers, and the experiments are relatively simple and efficient. However, a notable problem is that the experimental data for the adhesion energy of graphene/substrate systems are widely scattered. Even with the same method, the obtained adhesion energy could be quite different. There may be many possible causes for the scattered adhesion energy values, and one of them may be the effect of separation rate, which is the focus of the present study.

In this study, we focused on the measurement of adhesion energy between large-scale CVD graphene and a poly(ethylene terephthalate) (PET) substrate. To investigate the effect of the separation rate, the DCB tests were conducted at seven different separation rates, and the apparent adhesion energy was determined at each separation rate. After each DCB test, the 2D-peak-position (strain) field of the transferred graphene was measured and analyzed using in situ micro-Raman spectroscopy. Based on the Raman results, the effect of separation rate on the decohesion mode was discussed. Finally, an appropriate separation rate was proposed for dry transferring the graphene and measuring the adhesion energy of graphene without the influence of fracturing and straining the graphene.

## 2. Results and Discussions

### 2.1. Measurement of Apparent Adhesion Energy

To measure the adhesion energy of the monolayer graphene/PET interface, the DCB specimens were fabricated as shown in Figure 1, where the graphene-coated PET substrate was

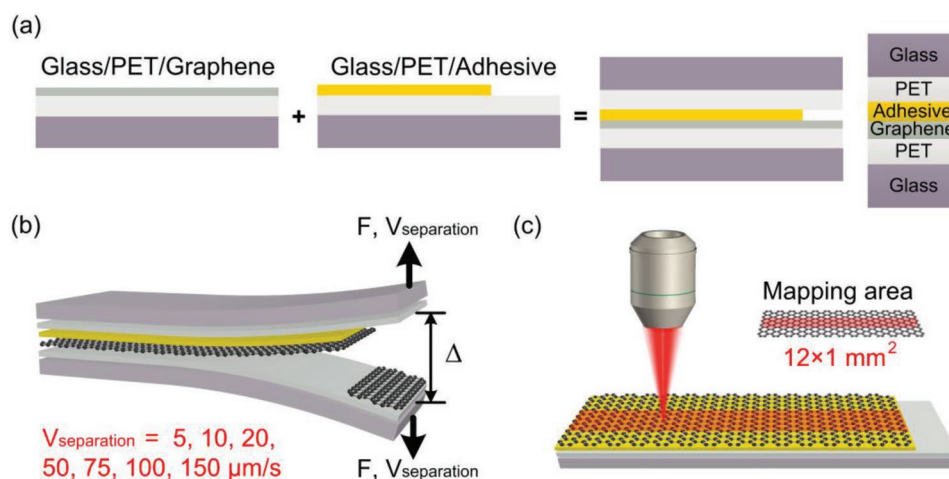


**Figure 1.** Schematic illustrations showing a) fabrication of the DCB specimens; b) specimen during DCB tests, with application of seven different separation rates; and c) micro-Raman mapping of the transferred graphene, with the mapping area highlighted by the red-shaded region (not to scale).

sandwiched between glass strips with ultraviolet (UV) epoxy used as an adhesive to form the glass/PET/graphene/adhesive/PET/glass laminated structure. The DCB specimen was 50 mm long and 5 mm wide. More experiment details are provided in the Experimental Section. We chose the polymer PET as the substrate for the following reasons. First, polymers are often used as the substrates in flexible electronic devices, a promising application area of 2D materials. Successful dry transfer of high-quality macrosized graphene to the polymer substrate is a key step in the fabrication process of these devices, especially the graphene heterostructure-based devices. Therefore, studying PET–graphene adhesion is of technical relevance. Second, as PET film is nearly atomically flat, using it as a substrate would help minimize the influence of roughness in the experiments. In our previous studies, we found that the dry transfer of graphene can be simultaneously affected by the roughness of substrate and the separation rate.<sup>[5,13,18]</sup> Third, PET is a typical polymeric materials widely adopted in flexible electronic devices. Studying the rate-effect helps provide a guideline for choosing the optimal separation rate in dry-transfer technique of graphene to various polymeric substrates.

The DCB specimens and the loading device are shown in Figure S1 (Supporting Information). Here, to determine the effect of the separation rate on the apparent adhesion energy of graphene, we performed a series of DCB tests using seven

separation rates of  $V_{\text{separation}} = 5, 10, 20, 50, 75, 100, 150 \mu\text{m s}^{-1}$ , as indicated in Figure 1b. After the DCB test, the transferred graphene on the adhesive was evaluated using micro-Raman spectroscopy. The in situ scanning mode of Raman mapping was applied to measure the strain distribution of the transferred graphene, as shown in Figure 1c.

The load–displacement response of the specimen during mechanical delamination (dry transfer) in the DCB test can be analyzed using the simple beam theory,<sup>[5,15]</sup> leading to a relationship between the applied peeling force ( $F$ ) and the opening displacement ( $\Delta$ ) as

$$F = \frac{Ebh^3\Delta}{8a^3} \quad (1)$$

where  $a$  is the crack length measured from the point of load application to the crack front, marked in the inset of Figure 2a. The other parameters in Equation (1),  $E$ ,  $b$ , and  $h$ , are, respectively, the in-plane Young's modulus (8 GPa), width (5 mm), and thickness (1 mm) of the glass strips. It is noted that the presence of PET, adhesive, and graphene between the glass strips has a negligible effect and hence has been ignored in the simple beam analysis. As indicated in Equation (1), the stiffness (or slope) of the load–displacement response depends on the crack length and should remain constant until the crack

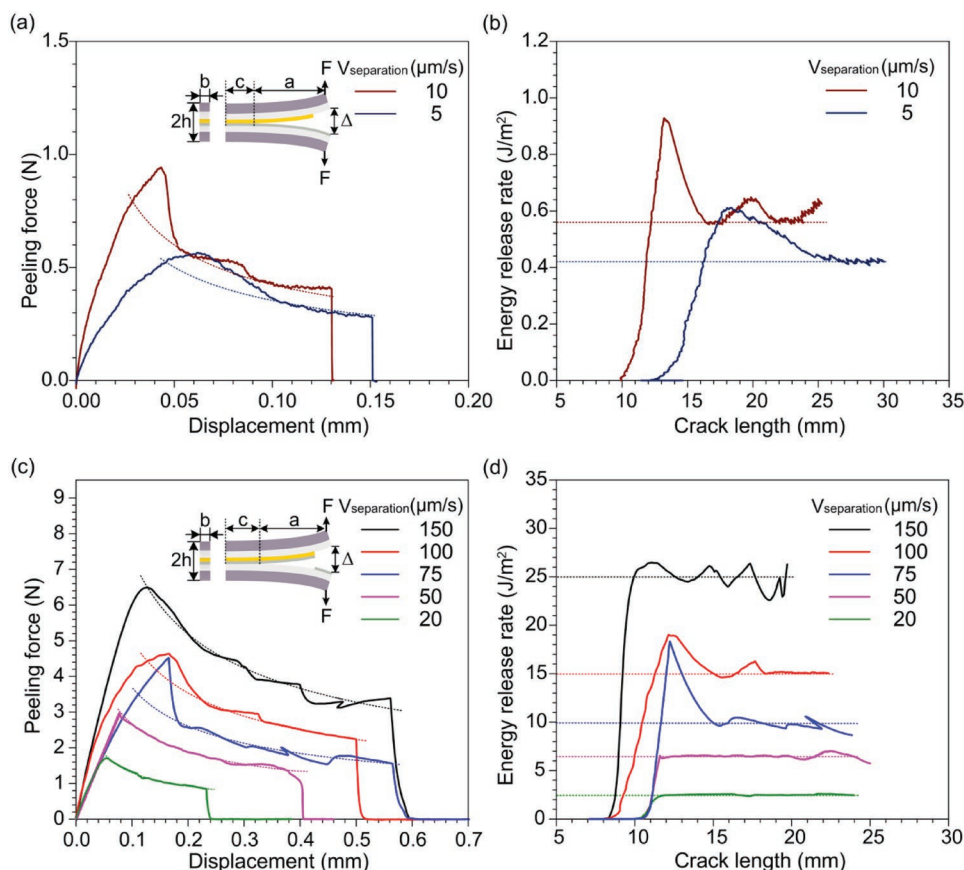


**Figure 2.** Force–displacement responses of DCB fracture tests with separation rates of a) 5, 10  $\mu\text{m s}^{-1}$  and c) 25–150  $\mu\text{m s}^{-1}$ . A schematic illustration of the DCB specimen is shown in the inset, and the measured mechanical parameters are marked. Delamination resistance curves for the graphene/adhesive interface with separation rates of b) 5, 10  $\mu\text{m s}^{-1}$  and d) 25–150  $\mu\text{m s}^{-1}$ .

grows. The crack length  $a$  can be determined from Equation (1) as

$$a = \sqrt[3]{\frac{Ebh^3\Delta}{8F}} \quad (2)$$

The driving force for delamination crack growth is the energy release rate ( $G$ ), which can also be determined using the simple beam theory and is given by

$$G = \frac{12a^2F^2}{Eb^2h^3} \quad (3)$$

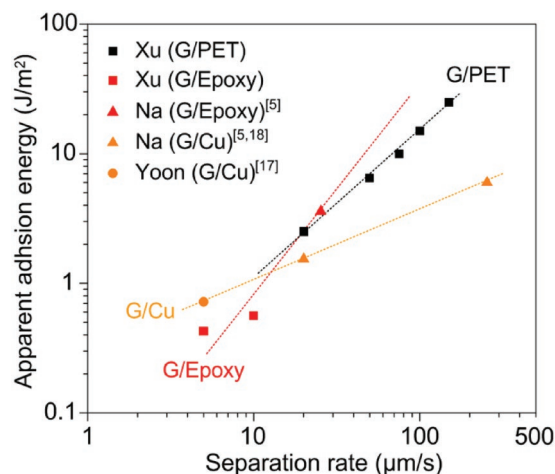
Thus, before the onset of delamination, the energy release rate increases with increasing applied displacement and the reaction force until crack growth initiates, after which the reaction force decreases as the crack length increases and the energy release rate remains a constant. By measuring the peeling force and the opening displacement (Figure 2a,c), the crack length  $a$  can be determined from Equation (2), and the fracture resistance curve ( $R$ -curve) can then be obtained by plotting the energy release rate as a function of the crack length for each specimen (Figure 2b,d). The  $R$ -curve typically exhibits an increase in the energy release rate followed by a plateau for steady-state crack growth at a constant energy release rate. An overshoot of the energy release rate was observed in some cases, which was likely due to a crack blunting effect.<sup>[21,22]</sup> In accordance with the energy criterion for delamination crack growth, the plateau energy release rate for steady-state delamination is taken as the apparent adhesion energy of the interface ( $\Gamma_a$ ). The subsequent load–displacement response largely follows  $G = \Gamma_a$ . The apparent adhesion energy was shown by the dotted lines in Figure 2b,d.

Figure 2a,b shows the force–displacement response and the delamination resistance curves for the DCB fracture tests with the separation rates of 5 and 10  $\mu\text{m s}^{-1}$ . For these two separation rates, the delamination occurred along the graphene/adhesive interface instead of the graphene/PET interface, indicating that the graphene was not transferred at the low separation rates. As a result, the adhesion energy of the graphene/PET interface could not be obtained at these rates. Instead, the apparent adhesion energy of the graphene/UV epoxy interface was obtained to be 0.42 and 0.56  $\text{J m}^{-2}$ . On the other hand, at the separate rates from 20 to 150  $\mu\text{m s}^{-1}$ , the delamination grew along the graphene/PET interface and the graphene was transferred from the PET substrate onto the adhesive. Our previous study observed similar results although with a different substrate material, i.e., the delamination path depended on the separation rates and graphene could not be transferred at relatively low separation rates.<sup>[5]</sup>

Figure 2c shows the measured force–displacement responses for the DCB fracture tests at the five separation rates greater than 10  $\mu\text{m s}^{-1}$ , and Figure 2d shows the corresponding delamination  $R$ -curves. In all these cases, the crack formed and grew along the graphene/PET interface, while the peeling force decreased gradually after a maximum. The maximum peeling force varied for the different DCB tests, depending on the separation rate as well as the initial crack length. The peeling force peaked at 6.6 and 1.6 N for separation rates of 150 and

20  $\mu\text{m s}^{-1}$ , respectively, indicating a difference of 4 times. Based on the delamination  $R$ -curves in Figure 2d, the apparent adhesion energy of the graphene/PET interface was obtained from the steady-state energy release rate for each separation rate, as depicted by the dashed lines in Figure 2d. The apparent adhesion energy of the graphene/PET interface increased by one order of magnitude, from 2.5 to 25  $\text{J m}^{-2}$ , as the separation rate increased from 20 to 150  $\mu\text{m s}^{-1}$ . These values are much higher than the estimated adhesion energy ( $\approx 0.54 \text{ J m}^{-2}$ ) by Jiang et al.<sup>[9]</sup> based on a buckle delamination method. It is noted that the energy release rate fluctuated slightly near a constant value even during the steady-state crack growth period, as shown in the Figure 2b,d, suggesting that the inhomogeneous factors, such as the grain boundaries, multilayer spots, and ripples of graphene could slightly affect the measurement of the apparent adhesion energy. However, because these defects are distributed randomly across the specimens with typical size scales up to tens of micrometers, while the decohesion process was measured at a macro scale (centimeter scale), the measured interfacial energy would be a homogenized value containing the influences of all these micro-sized defects, as the dashed lines shown in Figure 2b,d, and these micro-sized defects had limited influence on the overall trend of the rate-dependence.

For comparison, Figure 3 shows the measured apparent adhesion energy by DCB fracture tests as a function of the separation rate. The square data points were obtained from the experiments in the current study (Figure 2b,d); the circular point was obtained from Yoon et al. and the triangular points were obtained from our group's previous works by Na et al.<sup>[5,17,18]</sup> It is noted that the epoxy used in the current study was similar to that in the previous work by Na et al.,<sup>[5]</sup> where two values of adhesion energy were reported, one for the graphene/epoxy interface at 25.4  $\mu\text{m s}^{-1}$  and the other for graphene/Cu at 254  $\mu\text{m s}^{-1}$ . The data for the three types of interfaces (graphene/PET, graphene/epoxy, and graphene/Cu) in Figure 3 show that the apparent adhesion energy of each interface was dependent on the separation rate, increasing



**Figure 3.** Variation of measured adhesion energy by DCB fracture tests as a function of the separation rate. The square data points were obtained from the experiments in the current study; the circular and triangular data points were obtained from previous works.<sup>[5,17,18]</sup>

with the increase of separation rate. In the current study, the different decohesion modes at different separation rates reflect the competition between the two interfaces (graphene/PET and graphene/epoxy), as illustrated by the black and red dashed lines in Figure 3. When the separation rate was relatively low (less than  $20 \mu\text{m s}^{-1}$ ), the crack grew along the weaker graphene/epoxy interface (decohesion mode I), indicating that the adhesion energy of the graphene/PET interface was greater than that of the graphene/epoxy interface. On the other hand, when the separation rate was higher, the crack grew along graphene/PET interface instead (decohesion mode II) and thus the graphene/PET interface was weaker compared to that of the graphene/epoxy interface. It is noted that, in Yoon et al.'s case,<sup>[17]</sup> they measured the Cu/graphene/epoxy structure. They reported that the adhesion energy of graphene/Cu was  $0.72 \text{ J m}^{-2}$  for separation rates of  $5 \mu\text{m s}^{-1}$ , suggesting that the adhesion energy of graphene/epoxy they used should be larger than  $0.72 \text{ J m}^{-2}$ . It appeared that the adhesion energy of graphene/epoxy measured in Yoon et al.'s experiment was larger than that we measured ( $0.42\text{--}0.56 \text{ J m}^{-2}$ ). This discrepancy can potentially be caused by the different epoxy materials that were used in the experiments.

According to previous studies, the rate-dependent adhesion energy may be attributed to the viscoelasticity of the adhesive and PET substrate and the related crack tip blunting.<sup>[23–25]</sup> For a typical viscoelastic polymer, the adhesion energy increased linearly as a function of the separation rate in linear-log scale.<sup>[26–28]</sup> However, the data in Figure 3 exhibit a different rate-dependence, with the apparent adhesion energy increasing linearly with the increase of separation rate in log–log scale, thus a stronger rate effect than viscoelasticity. To shed light on the possible causes of the enhanced rate-dependence observed in

Figure 3, we conducted in situ micro-Raman spectroscopy on the transferred graphene searching for the decohesion mode III.

## 2.2. Evaluation of Transferred Graphene Using Raman Spectroscopy

In situ micro-Raman spectroscopy was employed here to measure the strain field of the transferred graphene on the adhesive layer. **Figure 4** presents Raman maps of the 2D peak position over the mapping area of graphene and histograms of the 2D peak position data before and after the DCB tests at separation rates of  $20\text{--}150 \mu\text{m s}^{-1}$ . As shown in the inset, the delamination crack along the graphene/PET interface propagated from right to left in the DCB test; therefore, the crack began at the right edge of the Raman maps. The bar legend shows the relationship between the contour colors and the 2D peak position, and if the area of the sampling point was not covered by graphene, the color white was used, indicating the fractured area (marked as “No G”). Raman maps in Figure 4a indicate that the quality of the transferred graphene varied significantly with separation rate. Herein, two parameters of the graphene coverage rate and the strain field uniformity were defined to quantitatively characterize the quality of the transferred graphene. First, we focus on the coverage rate of the transferred graphene, which was defined as the ratio of the area covered with graphene to the total adhesive area. The coverage rate for the various separation rates was calculated and shown in Figure 4b. The white columns in the histograms in Figure 4b show the ratio of the area not covered with graphene (No G) to the total adhesive area, so the coverage rate of the transferred graphene equaled 100% minus the percentage of

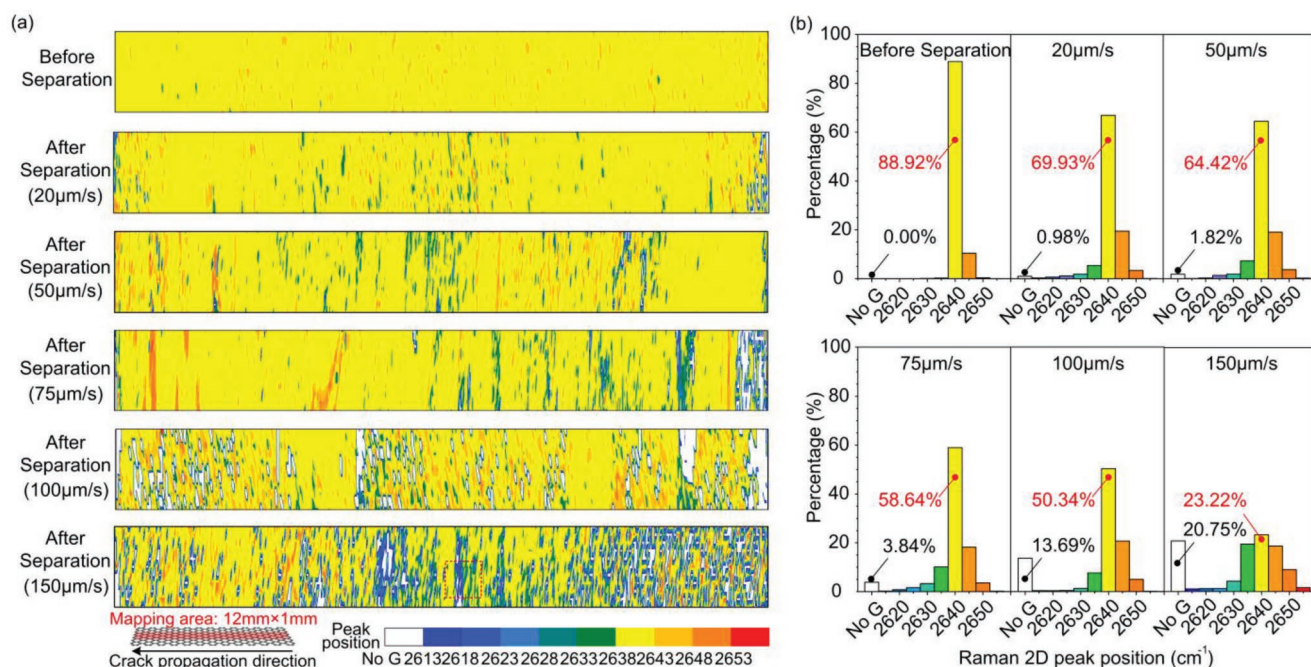


**Figure 4.** a) Raman maps of the 2D peak position over a  $12 \times 1 \text{ mm}^2$  mapping area of graphene before and after the DCB tests at separation rates of  $20\text{--}150 \mu\text{m s}^{-1}$  (not to scale). The red dashed square of  $500 \times 500 \mu\text{m}^2$  was enlarged in Figure 6. b) Histograms of the 2D peak position data of the graphene before and after the DCB tests.

the white column. As observed in the Raman map, before the DCB fracture test, the PET substrate was completely covered by graphene, which was intact. After the DCB fracture test at the separation rate of  $20 \mu\text{m s}^{-1}$ , the entire mapping area of the transferred graphene was colored, except for a few spots near the edge, suggesting that the graphene was largely transferred from the PET to the adhesive without fracturing at this separation rate, yielding a graphene coverage rate as high as 99.02% (0.98% fracture as shown in Figure 4b). Higher separation rates yielded more white areas in the map and thus a lower graphene coverage rate, especially for a separation rate greater than  $100 \mu\text{m s}^{-1}$ . After the DCB fracture test at the separation rate of  $150 \mu\text{m s}^{-1}$ , a large amount of white area appeared in the Raman map, indicating that the graphene was significantly fractured during the dry transfer. The fractured area was present throughout the mapping area of the transferred graphene. As a result, part of the graphene remained on the PET substrate and failed to be transferred. Therefore, the high separation rate led to the fracture of the graphene, and the coverage rate of the transferred graphene was only 79.25%. Moreover, the fractured area exhibits a banding distribution along the width direction, which was perpendicular to the peeling direction, especially at the center of the map; the fractured area spreads across the entire width of transferred graphene like a white stripe.

The strain field of the transferred graphene was also considered. Before the DCB test, the main color of the map was yellow, indicating that most of the 2D peak position was located at  $2640 \pm 2.5 \text{ cm}^{-1}$ ; hence,  $2640 \text{ cm}^{-1}$  was considered the reference 2D peak position at zero strain. A small portion of the mapping area was orange or green, indicating shifts of the 2D peak position due to residual strain. The residual strain was fairly small and localized in random spots, likely introduced by the poly (methyl methacrylate) (PMMA)-based wet-transfer process of graphene. After the graphene was peeled off the PET substrate at various separation rates, the 2D peak position field (the uniformity of the strain field) of the transferred graphene apparently changed. Herein, to characterize the uniformity of the strain field, the zero-strain graphene rate was defined as the ratio of the sampling points with zero strain (i.e., 2D peak position at  $2640 \pm 2.5 \text{ cm}^{-1}$ ) to the total number of sampling points. The zero-strain graphene rate for the various separation rates was shown by the yellow columns of the histograms in Figure 4b. After the graphene was transferred with a separation rate of  $20 \mu\text{m s}^{-1}$ , the 2D peak position (strain) field changes and spotted areas of blue and green colors appear, though the main color remains yellow. This suggests that part of the transferred graphene was subject to tension, whereby the zero-strain graphene rate decreased from 88.92% (before DCB test) to 69.93%. A higher separation rate led to a larger area of residual strain in the map and thus a lower zero-strain graphene rate. When the separation rate was  $150 \mu\text{m s}^{-1}$ , although the main color was still yellow, large areas of blue and dark blue appeared (the 2D peak position was decreased), suggesting that a significant part of the transferred graphene was subject to tension, especially in the region around the fractured area. As a result, the zero-strain graphene rate was only 23.22%. By contrast, the shift of 2D peak is much less in the transferred graphene by the separation rate of  $20 \mu\text{m s}^{-1}$ . The variation of the graphene coverage rate and the zero-strain graphene rate as a function of the separation rate is given in Figure 5.

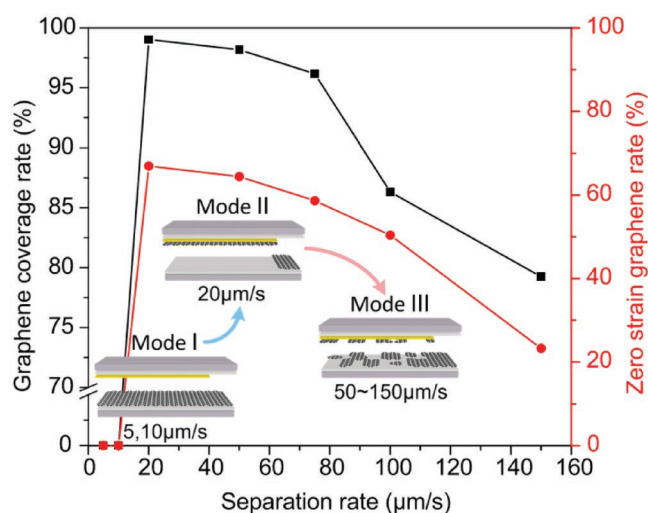


**Figure 5.** Coverage rate (left axis) and zero strain graphene rate (right axis) of the transferred graphene as a function of the separation rate. (Inset) Schematic of the three decohesion modes at varied separation mode.

To explore the fracture and residual tensile strain introduced in the transferred graphene, a  $500 \times 500 \mu\text{m}^2$  area in Figure 4 ( $150 \mu\text{m s}^{-1}$ ) was selected and enlarged, as shown in Figure 6. The 2D peak position is shown in Figure 6a. The white area where the graphene was fractured was encircled by the blue area of high residual tensile strain, suggesting that the residual tensile strain was closely related to the fracture of graphene. Since graphene produced by the CVD method is a 2D polycrystalline material, there are many weak links such as grain boundaries or defects. The PET substrate had the nanoscale roughness, so the graphene cannot completely conform to the morphology of the PET surface, and some regions of graphene may float on the PET, which gave rise to more weak points throughout the graphene. When the separation rate was high, the adhesion energy of the graphene/PET and the graphene/epoxy were thus high based on Figure 3, as a result, the two opposite forces caused the fracture of the weak areas of graphene during dry transfer, and the area surrounding the fractured area was subjected to irreversible residual tensile strain, which was detected by the Raman spectroscopy. The minimum value of the 2D peak position in Figure 6a was  $2615 \text{ cm}^{-1}$ ; if  $2640 \text{ cm}^{-1}$  was considered the zero strain and  $8 \text{ cm}^{-1} \%^{-1}$  was used as the Raman 2D shift to strain coefficient,<sup>[29]</sup> the maximum residual tensile strain of the transferred graphene was  $\approx 3\%$ . Because the graphene is expected to fracture when the tensile strain reaches the fracture limit of graphene, it may be estimated that the fracture limit of graphene produced by the CVD method was  $\approx 3\%$ .

To further explore the area of graphene with residual tensile strain, Figure 6b presents Raman maps of the full width at half maximum (FWHM), and four sampling points in Figure 6a,b were selected to compare the shape of the 2D peak. The state of graphene can be judged from the FWHM. The original shape of the 2D peak without any strain or damage was high and sharp, as indicated by point A in Figure 6c. Therefore, in Figure 6b, the area without strain has the minimum FWHM. When the graphene was subjected to tensile or compressive strain, the 2D peak intensity decreased, and the FWHM slightly increased, as

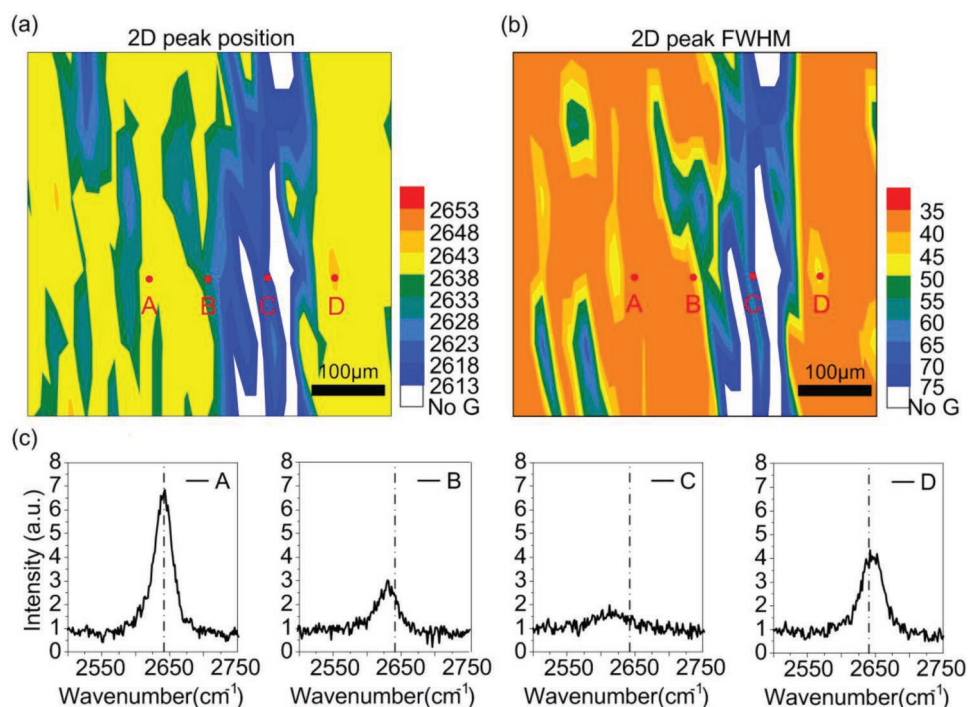


**Figure 6.** Raman maps of a) 2D peak position and b) full width at half maximum over a  $500 \times 500 \mu\text{m}^2$  mapping area of the graphene after the DCB test at the separation rate of  $150 \mu\text{m s}^{-1}$ . The scale bar was  $100 \mu\text{m}$ . c) Raman 2D peak of graphene at four sampling points in (a) and (b). The dashed line indicates the initial peak position at  $2640 \text{ cm}^{-1}$ .

indicated by points B and D. However, when the graphene was damaged, the FWHM of the 2D peak sharply increased, as indicated by point C.<sup>[30]</sup> Combining Figure 6a,b, the blue area with large residual tensile strain in Figure 6a corresponded to the blue area with damage in Figure 6b, indicating that the damage of graphene was accompanied by large residual strain, and the fractured areas were always surrounded by the damaged area. This experimental result agreed with the simulations by Zhang et al.<sup>[31]</sup> and Fan et al.<sup>[32]</sup> developed finite element models of graphene strips to predict dynamic fracture. The crack instability and branching were observed in their simulations, and they found that the crack edges were irregular accompanied with oscillatory overhangs, topological defects, and carbon chain bridging. Their simulations also indicated that the level of damage (kinking and oscillation occurred around the crack) was related to the loading rates. Figure 6 shows that in the DCB test, a high separation rate led to delamination of the graphene/PET interface along with fracture of the transferred graphene and damage in the area surrounding the fracture. In addition, the damaged graphene was accompanied by the appearance of residual tensile strain of up to 3%. Therefore, decohesion mode III appeared in the sandwich specimen if the separation rate was high during dry transfer, as shown in the inset of Figure 5.

### 2.3. Discussions on Rate-Dependence of Decohesion Mode and Adhesion Energy

**Table 1** summarizes the experimental results of the DCB fracture tests for the seven applied separation rates, including the apparent

adhesion energy, the decohesion mode, and the quality of the transferred graphene. The results indicate that graphene was not peeled off the PET substrate at a separation rate of  $10 \mu\text{m s}^{-1}$  or lower. The adhesion energy of the graphene/PET interface could not be obtained in these cases; instead, the adhesion energy of the graphene/UV epoxy interface was obtained. As indicated in Figure 3, it is expected that the adhesion energy of the graphene/PET interface was higher than that of the graphene/adhesive at the relatively low separation rate so that the delamination occurred along the weaker graphene/epoxy interface (decohesion mode I). On the other hand, with higher separation rates, the adhesion energy of the graphene/PET interface was lower than that of the graphene/adhesive, and the delamination path changed to the graphene/PET interface (decohesion mode II). The results in Table 1 indicate that the graphene was partly transferred but fractured and strained at a separation rate of  $50 \mu\text{m s}^{-1}$  or higher and the graphene uniformity was reduced to various degrees with various separation rates (decohesion mode III). In addition to the Raman mapping method, the quality of the transferred graphene was also confirmed by the electrometric method (see Figure S2 in the Supporting Information). Both low and intermediate rates may be useful for selective dry transfer: first transfer the graphene to the adhesive by an intermediate rate (not too high to avoid the appearance of decohesion mode III) and then release the graphene from the adhesive by a low rate to a target substrate. In this case, a separation rate of  $20 \mu\text{m s}^{-1}$  was most suitable for the complete dry transfer of graphene from PET substrate with better integrity and uniformity. Therefore, this study provided a reference for dry transferring high-quality graphene or other nanofilms in heterostructure-based electronic devices.

**Table 1.** Summary of the DCB tests at different separation rates.

Separation rate [ $\mu\text{m s}^{-1}$ ]	Decohesion mode	Apparent adhesion energy [ $\text{J m}^{-2}$ ]	Graphene coverage rate [%]	Zero-strain graphene rate [%]
Before Separation	–	–	100	88.92
5	Delamination (G/epoxy)	0.42	0	0
10	Delamination (G/epoxy)	0.56	0	0
20	Delamination (G/PET)	2.5	99.02	69.93
50	Delamination (G/PET) + fracture (G) + residual strain (G)	6.5	98.18	64.42
75	Delamination (G/PET) + fracture (G) + residual strain (G)	10	96.16	58.64
100	Delamination (G/PET) + fracture (G) + residual strain (G)	15	86.31	50.34
150	Delamination (G/PET) + fracture (G) + residual strain (G)	25	79.25	23.22

Based on the Raman analysis and Table 1, we found that, for a high separation rate, the delamination along the graphene/PET interface was accompanied by fracture of the graphene and that the transferred graphene was strained and damaged around the fractured areas. The fracture and damage of graphene dissipated extra energy, which led to higher apparent adhesion energy as measured by the DCB tests. In addition, the high separation rate led to a residual tensile strain of up to 3% in the transferred graphene; hence, the residual strain energy of graphene could also contribute to the apparent adhesion energy.

Therefore, the energy criterion for the delamination crack growth along the graphene/PET interface should be modified to include the additional energy dissipation caused by the fracture and residual strain. Herein, we considered that the apparent adhesion energy (plateau energy release rate) measured in the DCB test was balanced by the following three parts

$$\Gamma_a = \Gamma_i + W_{\text{fra}} + W_{\text{res}} \quad (4)$$

where  $\Gamma_i$  is the intrinsic adhesion energy of the interface,  $W_{\text{fra}}$  and  $W_{\text{res}}$  are the energy associated with fracture and residual strain of graphene, respectively. Based on the Raman analysis above,  $W_{\text{fra}}$  and  $W_{\text{res}}$  were obviously rate-dependent and according to previous researches, the intrinsic adhesion energy of the interface  $\Gamma_i$  was rate-dependent either. It has long been observed that adhesion of polymer interfaces possesses significant rate-dependence. This particular effect has been attributed to viscoelasticity and crack tip blunting during interface decohesion, which could be further traced to the molecular scale viscosity of polymeric interactions.<sup>[23–25]</sup> For example, Gent<sup>[24]</sup> indicated that the energy release rate (adhesion energy) of interfacial area was a product of two terms, one was the intrinsic strength of the interface and the other reflected energy dissipated viscoelastically at specific separation  $R$  and temperature  $T$ . The dry transfer of graphene by DCB method was a thermally activated bond breaking process, which could be influenced by loading history (i.e., separation rates).<sup>[33]</sup> In ref. [34], a stochastic description about the mechanical response of an interface composed of noncovalent bonds was proposed, where the evolution of bonding probability in response to deformation plays the central role in determining their traction–separation behavior. Based on such theory, they found that the strong rate sensitivity of released energy as they separated the interface at

higher rates, with more energy required at faster separation rate.<sup>[34]</sup> The proposed theoretical model agreed well with the rate-dependency observed in our experiment, and such stochastic noncovalent bond rupture kinetics of graphene interface can be one of the main causes for the rate-dependence. Therefore, all three energy terms in Equation (4) may depend on the separation rate; as a result, the measured apparent adhesion energy  $\Gamma_a$  exhibited the enhanced rate-dependence in the DCB tests. Hence, the intrinsic adhesion energy is

$$\Gamma_i(v) = \Gamma_a(v) - W_{\text{fra}}(v) - W_{\text{res}}(v) \quad (5)$$

To measure the intrinsic adhesion energy of the graphene/PET interface, the effect of the fracture energy and residual strain energy of graphene should be eliminated as much as possible. In this study, when the DCB test was performed at the separation rate of  $20 \mu\text{m s}^{-1}$ , the graphene was completely peeled off the PET substrate without significant fracture or residual strain. In this case, the apparent adhesion energy measured in Figure 2 can be considered the intrinsic adhesion energy of the graphene/PET interface, i.e.,  $\Gamma_i \approx \Gamma_a = 2.5 \text{ J m}^{-2}$ . In other cases, the apparent adhesion energy would involve fracture and residual energy of graphene, so cannot be considered as the intrinsic adhesion energy. Therefore, an appropriate method for determining the intrinsic adhesion energy of the interface between graphene and the substrate is proposed. The lowest separation rate that can be used to peel the graphene off the substrate should be applied in the DCB test to avoid the appearance of the decohesion mode III. In this way, the effect of the extra contributions from the fracture energy and residual strain energy of graphene can be eliminated as much as possible, and an accurate measurement of the adhesion energy can be obtained.

### 3. Conclusion

The adhesion energy is an important parameter characterizing the strength of the graphene/substrate interface and its characterization has widespread significance for the fabrication of graphene-based devices. By conducting DCB fracture tests with different separation rates, we measured the apparent adhesion energy of the sandwiched adhesive/graphene/PET interface. The experimental results showed that both the decohesion



mode and the apparent adhesion energy of the graphene-sandwiched interface were strongly rate-dependent. When the separation rate was relative low, decohesion occurred at the graphene/adhesive interface (mode I). By contrast, peeling at an intermediate separation rate would result in delamination along the graphene/PET interface with graphene being dry transferred to the adhesive (mode II). When separation rate was further increased, the transferred graphene was locally fractured and damaged containing a significant level of residual tensile strain (mode III). This phenomenon was contrary to earlier reports, where higher separation rate would typically enhance the dry transfer of graphene resulting in better integrity and performance. The new decohesion mode III appeared in dry transfer and the transition in decohesion modes led to enhanced rate-dependency of the measured apparent adhesion energy due to extra energy dissipation associated with the local fracture and the residual straining of graphene, and the apparent adhesion energy measured in the DCB tests may not be an intrinsic property of the interface. For accurate measurement of the intrinsic graphene/PET adhesion energy, the effect of fracture and residual strain of graphene should be minimized as much as possible. Furthermore, the different decohesion modes revealed by this work, especially the new decohesion mode appeared in dry transfer with high separation rate, provide a guideline for choosing the optimal separation rate in dry-transfer technique of graphene to obtain samples with better integrity and uniformity.

#### 4. Experimental Section

**Sample Preparation:** Monolayer polycrystalline graphene was synthesized on copper foil using chemical vapor deposition and had dimensions of 20 mm in length and 5 mm in width. The CVD graphene contained some multilayer spots, as shown by the dark spots in Figure S1 (Supporting Information). However, the percentage of the monolayer graphene was larger than 95%, which was determined by the Raman microscopy in Figure S3 (Supporting Information). The PET substrate was 50 mm long, 5 mm wide, and 0.1 mm thick. The monolayer graphene film was transferred to the top surface of the PET substrate using the PMMA-assisted wet transfer method. To measure the adhesion energy of the graphene/PET interface, the DCB specimens were fabricated as shown in Figure 1, where the graphene-coated PET substrate was sandwiched between glass strips with UV epoxy used as an adhesive to form the glass/PET/graphene/adhesive/PET/glass laminated structure. The DCB specimen was 50 mm long and 5 mm wide. Microbubbles might form during the sample preparation. To minimize the influence, two measures were employed. First, the adhesive was degassed in a vacuum chamber before making specimens. Second, the HR-3362 UV epoxy was selected as the adhesive because of its higher solvent stability, stronger adhesion force, and higher conformal contact with graphene compared to the normal epoxies.<sup>[35]</sup> Meanwhile, the impact of the gentle UV exposure process in the sample preparation was minimal. At low separation rate, the entire graphene was transferred from the PET to the adhesive without fracturing. In this case, the Raman spectra suggested that the graphene was intact even after the UV exposure process. Since a same protocol was used for all samples, it was assumed that the UV exposure would not induce noticeable defects in graphene. Similar behavior was reported in an earlier study using UV epoxy as a transfer medium.<sup>[35]</sup> The adhesive was applied evenly on the PET, as depicted by the yellow area in Figure 1a, and the size of the covered area was ≈12 mm long by 5 mm wide. The actual length varied slightly because of the mobility of the UV epoxy; therefore, the length

of the transferred graphene also slightly varied. Here, to determine the effect of the separation rate of the dry transfer on the adhesion energy of graphene, a series of DCB tests were performed using seven separation rates of  $V_{\text{separation}} = 5, 10, 20, 50, 75, 100, 150 \mu\text{m s}^{-1}$ , as indicated in Figure 1b. Because the roughness of the substrate surface could be another factor affecting the adhesion energy, the PET substrates used in the experiments and all the other experimental conditions were kept nearly identical. The DCB specimens and the loading device are shown in Figure S1 (Supporting Information).

**Micro-Raman Measurements:** Micro-Raman spectroscopy is one of the most effective methods to study the properties of graphene because it is a nondestructive, noncontact, and rapid technique with high spatial resolution (≈1 μm) and enables quantitative measurement of mechanical parameters. The measurement principle was based on the change in the atomic bond length caused by strain of the graphene lattice, leading to change in the frequency of lattice vibrations (phonons) and a corresponding shift of the characteristic peak frequency in Raman spectrum.<sup>[36]</sup> Strain measurements for materials such as porous silicon materials, carbon nanotubes, and graphene were previously developed using Raman spectroscopy.<sup>[37–40]</sup> The detailed methodology of Raman mechanical measurements of graphene was shown in Figure S3 (Supporting Information). In the current study, after the dry transfer, the transferred graphene on the adhesive was evaluated using micro-Raman spectroscopy. The in situ scanning mode of Raman mapping was applied to measure the strain distribution of transferred graphene, as shown in Figure 1c. The red shaded area was the mapping area; the length was the real length of the transferred graphene, which was ≈12 mm; and the width was 1 mm. The mapping step was set to be 20 μm with a high Raman spatial resolution of ≈1 μm.

#### Supporting Information

Supporting Information is available from the Wiley Online Library or from the author.

#### Acknowledgements

This work was financially supported by the National Natural Science Foundation of China (Grant Nos. 11890683, 11672203, and 11827802) and the State Scholarship Fund from China Scholarship Council. T.Y., K.M.L., and R.H. gratefully acknowledge partial support by the Semiconductor Research Corporation (Task ID 2886.001).

#### Conflict of Interest

The authors declare no conflict of interest.

#### Keywords

adhesion, decohesion mode, graphene, Raman spectroscopy, rate effect

Received: July 15, 2019  
Revised: September 11, 2019  
Published online:

- [1] H. Kim, J. H. Ahn, *Carbon* **2017**, *120*, 244.
- [2] J. J. Park, W. J. Hyun, S. C. Mun, Y. T. Park, O. O. Park, *ACS Appl. Mater. Interfaces* **2015**, *7*, 6317.
- [3] S. Lee, S. H. Lee, T. H. Kim, M. Cho, J. B. Yoo, T. I. Kim, Y. Lee, *ACS Appl. Mater. Interfaces* **2015**, *7*, 8070.

- [4] J. Y. Moon, S. I. Kim, S. K. Son, S. G. Kang, J. Y. Lim, D. K. Lee, B. Ahn, D. Whang, H. K. Yu, J. H. Lee, *Adv. Mater. Interfaces* **2019**, *6*, 1900084.
- [5] S. R. Na, J. W. Suk, L. Tao, D. Akinwande, R. S. Ruoff, R. Huang, K. M. Liechti, *ACS Nano* **2015**, *9*, 1325.
- [6] Z. H. Ni, T. Yu, Y. H. Lu, Y. Y. Wang, Y. P. Feng, Z. X. Shen, *ACS Nano* **2008**, *2*, 2301.
- [7] S. R. Na, X. Wang, R. D. Piner, R. Huang, C. G. Willson, K. M. Liechti, *ACS Nano* **2016**, *10*, 9616.
- [8] L. Gong, I. A. Kinloch, R. J. Young, I. Riaz, R. Jalil, K. S. Novoselov, *Adv. Mater.* **2010**, *22*, 2694.
- [9] T. Jiang, R. Huang, Y. Zhu, *Adv. Funct. Mater.* **2014**, *24*, 396.
- [10] C. Xu, T. Xue, W. Qiu, Y. Kang, *ACS Appl. Mater. Interfaces* **2016**, *8*, 27099.
- [11] S. P. Koenig, N. G. Boddeti, M. L. Dunn, J. S. Bunch, *Nat. Nanotechnol.* **2011**, *6*, 543.
- [12] G. Wang, Z. Dai, Y. Wang, P. Tan, L. Liu, Z. Xu, Y. Wei, R. Huang, Z. Zhang, *Phys. Rev. Lett.* **2017**, *119*, 036101.
- [13] H. Xin, R. Borduin, W. Jiang, K. M. Liechti, W. Li, *Carbon* **2017**, *123*, 243.
- [14] Z. Cao, P. Wang, W. Gao, L. Tao, J. W. Suk, R. S. Ruoff, D. Akinwande, R. Huang, K. M. Liechti, *Carbon* **2014**, *69*, 390.
- [15] Z. Cao, L. Tao, D. Akinwande, R. Huang, K. M. Liechti, *J. Appl. Mech.* **2015**, *82*, 081008.
- [16] Z. Cao, L. Tao, D. Akinwande, R. Huang, K. M. Liechti, *Int. J. Solids Struct.* **2016**, *84*, 147.
- [17] T. Yoon, W. C. Shin, T. Y. Kim, J. H. Mun, T. S. Kim, B. J. Cho, *Nano Lett.* **2012**, *12*, 1448.
- [18] S. R. Na, S. Rahimi, L. Tao, H. Chou, S. K. Ameri, D. Akinwande, K. M. Liechti, *Nanoscale* **2016**, *8*, 7523.
- [19] J. W. Suk, S. R. Na, R. J. Stromberg, D. Stauffer, J. Lee, R. S. Ruoff, K. M. Liechti, *Carbon* **2016**, *103*, 63.
- [20] T. Jiang, Y. Zhu, *Nanoscale* **2015**, *7*, 10760.
- [21] A. J. Kinloch, J. G. Williams, *J. Mater. Sci.* **1980**, *15*, 987.
- [22] J. M. Hodgkinson, J. G. Williams, *J. Mater. Sci.* **1981**, *16*, 50.
- [23] X. Feng, M. A. Meitl, A. M. Bowen, Y. Huang, R. G. Nuzzo, J. A. Rogers, *Langmuir* **2007**, *23*, 12555.
- [24] M. A. Meitl, Z. T. Zhu, V. Kumar, K. J. Lee, X. Feng, Y. Y. Huang, I. Adesida, R. G. Nuzzo, J. A. Rogers, *Nat. Mater.* **2006**, *5*, 33.
- [25] A. N. Gent, *Langmuir* **1996**, *12*, 4492.
- [26] P. Rahulkumar, A. Jagota, S. J. Bennisson, S. Saigal, *Int. J. Solids Struct.* **2000**, *37*, 1873.
- [27] D. B. Xu, C. Y. Hui, E. J. Kramer, *J. Appl. Phys.* **1992**, *72*, 3305.
- [28] B. N. J. Persson, E. A. Brener, *Phys. Rev. E* **2005**, *71*, 036123.
- [29] H. Du, T. Xue, C. Xu, Y. Kang, W. Dou, *Opt. Lasers Eng.* **2018**, *110*, 356.
- [30] J. B. Wu, M. L. Lin, X. Cong, H. N. Liu, P. H. Tan, *Chem. Soc. Rev.* **2018**, *47*, 1822.
- [31] B. Zhang, H. F. Xiao, G. Yang, X. M. Liu, *Eng. Fract. Mech.* **2015**, *141*, 111.
- [32] N. Fan, Z. Ren, G. Jing, J. Guo, B. Peng, H. Jiang, *Materials* **2017**, *10*, 164.
- [33] T. Yang, X. Yang, R. Huang, K. M. Liechti, *J. Mech. Phys. Solids* **2019**, *131*, 1.
- [34] Y. Wei, *J. Mech. Phys. Solids* **2014**, *70*, 227.
- [35] L. P. Ma, S. Dong, M. Chen, W. Ma, D. Sun, Y. Gao, T. Ma, H. M. Cheng, W. Ren, *ACS Appl. Mater. Interfaces* **2018**, *10*, 40756.
- [36] W. Qiu, Y. L. Kang, *Chin. Sci. Bull.* **2014**, *59*, 2811.
- [37] C. Xu, T. Xue, J. Guo, Q. Qin, S. Wu, H. Song, H. Xie, *J. Appl. Phys.* **2015**, *117*, 164301.
- [38] C. Xu, T. Xue, J. Guo, Y. Kang, W. Qiu, H. Song, H. Xie, *Mater. Lett.* **2015**, *161*, 755.
- [39] W. Qiu, Q. Li, Z. K. Lei, Q. H. Qin, W. L. Deng, Y. L. Kang, *Carbon* **2013**, *53*, 161.
- [40] Y. L. Kang, Y. Qiu, Z. Lei, M. Hu, *Opt. Lasers Eng.* **2005**, *43*, 847.